Inorganic Chemistry
Article

Inorg. Chem. **2009**, *48*, 8393–8403 **8393**
DOI: 10.1021/ic901093c

Influence of Sulf-Oxygenation on CO/L Substitution and $Fe(CO)_3$ Rotation in Thiolate-Bridged Diiron Complexes

Bin Li,[†,‡] Tianbiao Liu,[†] Michael L. Singleton,[†] and Marcetta Y. Darensbourg*[,†]

[†]*Department of Chemistry, Texas A&M University, College Station, Texas 77843, and* [‡]*School of Chemical Engineering and Technology, Tianjin University, Tianjin 300072, P.R. China*

Received June 5, 2009

Kinetic studies of CO/L substitution reactions of the well-known organometallic complex (μ-pdt)[$Fe(CO)_3$]$_2$ (pdt = 1,3-propanedithiolate), complex **1**, and its sulfur−oxygenated derivative (μ-pst)[$Fe(CO)_3$]$_2$ (pst = 3-sulfenatopropane-1-thiolate), **1-O**, have been carried out with the goal of understanding the influence of the sulfenato ligand on the activation barrier to ligand substitution in such diiron carbonyl complexes which consists of two components: intramolecular structural rearrangement (or fluxionality) and nucleophilic attack by the incoming ligand. The CO/PMe_3 substitution reactions of complex **1** follow associative mechanisms in both the first and the second substitutions; the second substitution is found to have a higher activation barrier for the overall reaction that yields **1**-$(PMe_3)_2$. Despite the increased electrophilicity of the $Fe(CO)_3$ unit in **1-O** versus **1**, the former reacts more sluggishly with PMe_3, where practical kinetic measurements are at such high temperatures that CO dissociation parallels the associative path. Kinetic studies have established that in complex **1-O** both the first and the second CO/CN^- substitutions proceed via associative paths with higher E_{act} barriers than the analogous reactions with complex **1**. Theoretical calculations (density functional theory) have been used in conjunction with variable temperature ^{13}C NMR spectral studies to examine the energy barriers associated with rotation of the $Fe(CO)_3$ unit. The activation energy required for rotation is higher in the sulfenato than in the analogous thiolato complexes. Thus, the greater barrier to structural deformation in **1-O** inhibits its ability to expand its coordination number as compared to the thiolate, **1**, resulting in slower reaction rates of both PMe_3 and CN^- substitution reactions.

Introduction

Synthetic analogues of the dithiolate bridged diiron unit developed by nature to be a critical component of the active site of the all iron hydrogenase, [FeFe]H_2ase, provide an opportunity to explore the influences of specific changes on the fundamental properties of dinuclear complexes in general. One such property in (μ-pdt)[$Fe(CO)_3$]$_2$, a popular starting point for biomimetics, is the intramolecular CO_{ap}/CO_{ba} site exchange that occurs on individual iron centers, Scheme 1.[1,2] The barrier to this site exchange is a transition state whose computationally derived structure is an edge-bridged square pyramid/inverted square pyramid that mimics the "rotated" geometry of the active site.[3,4] Thus, as compared to the all-CO precursor complex, (μ-pdt)[$Fe(CO)_3$]$_2$, the effect of CN^-/CO replacement was to lower the barrier to $Fe(CO)_3$ rotation in (μ-pdt)[$Fe(CO)_3$]-[$Fe(CO)_2CN$]$^-$ through stabilization of the transition state via formation of a semi-bridging carbonyl, Scheme 1.[2,3]

Earlier we concluded that rates of CO/CN^- ligand substitution processes correlate with fluxionality in the $Fe(CO)_3$ rotors, that is, the intramolecular site exchange described above.[1] The reaction of (μ-pdt)[$Fe(CO)_3$]$_2$ with a cyanide salt, even with a deficiency of CN^-, resulted in the dicyano complex (μ-pdt)[$Fe(CO)_2(CN)$]$_2^{2-}$.[1] To isolate the monocyanide, (μ-pdt)[$Fe(CO)_3$][$Fe(CO)_2CN$]$^-$, the Na^+[$N(SiMe_3)_2$]$^-$ reagent was used to convert a single CO into CN^- through nucleophilic attack and elimination of $O(SiMe_3)_2$.[1] In this way, kinetic studies of sequential CO/CN^- substitution processes were possible. Each reaction was found to follow a second order rate expression, with $k_2' > k_2$, Scheme 2. As the second nucleophilic attack of CN^- was expected to be depressed by the anionic charge on (μ-pdt)-[$Fe(CO)_3$][$Fe(CO)_2CN$]$^-$, we proposed that the activation barrier must be apportioned into two contributory factors, defined in Figure 1.[2] The lower barrier of the second CO/CN^- substitution in Scheme 2 resulted from the smaller contribution to the activation barrier from the rotation of the unsubstituted $Fe(CO)_3$ unit which overwhelmed the increase in barrier due to nucleophilic attack.

*To whom correspondence should be addressed. E-mail: marcetta@mail.chem.tamu.edu.

(1) Lyon, E. J.; Georgakaki, I. P.; Reibenspies, J. H.; Darensbourg, M. Y. *J. Am. Chem. Soc*. **2001**, *123*, 3268–3278.
(2) Darensbourg, M. Y.; Lyon, E. J.; Zhao, X.; Georgakaki, I. P. *Proc. Natl. Acad. Sci. U.S.A*. **2003**, *100*, 3683–3688.
(3) Georgakaki, I. P.; Thomson, L. M.; Lyon, E. J.; Hall, M. B.; Darensbourg, M. Y. *Coord. Chem. Rev*. **2003**, *238*−*239*, 255–266.
(4) Tye, J. W.; Darensbourg, M. Y.; Hall, M. B. *Inorg. Chem*. **2006**, *45*, 1552–1559.

Published on Web 08/07/2009

Scheme 1. Intramolecular CO-Site Exchange (E_{act} values from DFT calculations.[3])

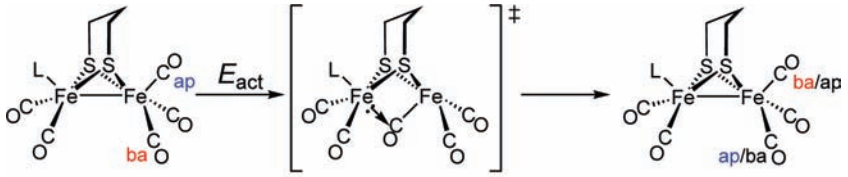

$L = CN^-$, $E_{act} = 3.9$ kcal/mol

$L = CO$, $E_{act} = 13.7$ kcal/mol

Scheme 2. Sequential CN^-/CO Substitution

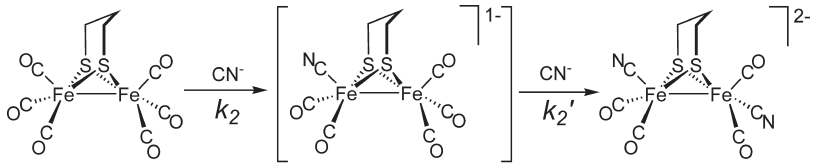

$k_2' > k_2$

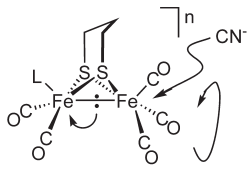

$E_{act}(\text{overall}) = E_{act}(CN^- \text{ attack}) + E_{act}(\text{rot'n})$

$E_{act}(CN^-$ attack)		E_{act}(rot'n)	
L = CO	<	$L = CN^-$	$L = CN^-$ < L = CO

Figure 1. Representation of events along the reaction coordinate for cyanide nucleophilic attack on diiron carbonyl, L = CO or CN^-, $n = 0$ or -1, and the equation describing contributing factors to the overall activation energy barrier.

Myriad derivatives of the (μ-pdt)[Fe(CO)$_3$]$_2$ complex have been prepared via CO/L substitution, replacement of the bridgehead C in the pdt by NR, O, S, Se,[5−10] steric modification by introducing substituents on the bridgehead C,[11] and replacement of the S donors by Se.[12] All such adaptations result in subtle differences in reactivity or redox properties. During recent studies of the S-oxygenate, (μ-pst)[Fe(CO)$_3$]$_2$ complex, we noted that while phosphines did not extract oxygen from the sulfenato sulfur, they displaced CO ligands at elevated temperatures as compared to the (μ-pdt)[Fe(CO)$_3$]$_2$ complex.[13] Thus the following kinetic studies of CO substitution by phosphines as well as cyanide were pursued in attempts to further test the mechanistic proposals above, as well as to establish the effect of the sulfenato group on the fluxionality and reactivity of the diiron complex. The complexes in this study and their abbreviations to be used hereafter are shown in Chart 1. Experimental values of Fe−Fe bond distance are given where available;[13−16] those in parentheses are density functional theory (DFT) calculated values.[13]

Experimental Section

Materials and Techniques. All reactions and operations were carried out on a double manifold Schlenk vacuum line under N_2 atmosphere. Hexane, CH_2Cl_2, CH_3CN, toluene, MeOH and diethyl ether were freshly purified on an MBraun Manual Solvent Purification System packed with Alcoa F200 activated alumina desiccant. The purified solvents were stored over molecular sieves under N_2 for no more than 1 week before use. The known complexes including (μ-pdt)[Fe(CO)$_3$]$_2$ (**1**),[1] (μ-pst)[Fe(CO)$_3$]$_2$ (**1-O**)[13] and (μ-pdt)[Fe(CO)$_3$][Fe(CO)$_2$PMe$_3$] (complex **1-PMe$_3$**)[17] were prepared according to literature procedures. The following materials were of reagent grade and were used as purchased from Sigma-Aldrich: $Fe_3(CO)_{12}$, 1,3-propanedithiol, trimethylphosphine, 3-chloroperoxybenzoic acid (purity 70−75%), $Et_4N^+CN^-$. Kinetic measurements using solution IR spectroscopy were carried out and recorded on a Bruker Tensor 27 FTIR spectrometer using 0.1 mm NaCl sealed cells. All NMR spectra were measured on a Varian Mercury or Unity +300 MHz NMR spectrometer. Variable temperature ^{13}C NMR spectra were collected on natural abundance samples using a Unity +500 MHz superconducting NMR instrument operating at 125.9 MHz

[Et$_4$N]{(μ-pst)[Fe(CO)$_3$][Fe(CO)$_2$CN]} (1-O-CN$^-$). To a solution of complex **1-O** (402 mg, 1.0 mmol) in 10 mL of CH_3CN was added a solution of $Et_4N^+CN^-$ (156 mg, 1.0 mmol) in 10 mL of CH_3CN; the reaction mixture was heated to 60 °C and

(5) Li, H.; Rauchfuss, T. B. *J. Am. Chem. Soc.* **2002**, *124*, 726–727.
(6) Wang, Z.; Liu, J.-H.; He, C.-J.; Jiang, S.; Akermark, B.; Sun, L.-C. *J. Organomet. Chem.* **2007**, *692*, 5501–5507.
(7) Windhager, J.; Rudolph, M.; Bräutigam, S.; Görls, H.; Weigand, W. *Eur. J. Inorg. Chem.* **2007**, *2007*, 2748–2760.
(8) Song, L.-C.; Yang, Z.-Y.; Bian, H.-Z.; Liu, Y.; Wang, H.-T.; Liu, X.-F.; Hu, Q.-M. *Organometallics* **2005**, *24*, 6126–6135.
(9) Song, L.-C.; Yang, Z.-Y.; Hua, Y.-J.; Wang, H.-T.; Liu, Y.; Hu, Q.-M. *Organometallics* **2007**, *26*, 2106–2110.
(10) Windhager, J.; Görls, H.; Petzold, H.; Mloston, G.; Linti, G.; Weigand, W. *Eur. J. Inorg. Chem.* **2007**, *2007*, 4462–4471.
(11) Singleton, M. L.; Jenkins, R. M.; Klemashevich, C. L.; Darensbourg, M. Y. *C. R. Chim.* **2008**, *11*, 861–874.
(12) Harb, M. K.; Niksch, T.; Windhager, J.; Görls, H.; Holze, R.; Lockett, L. T.; Okumura, N.; Evans, D. H.; Glass, R. S.; Lichtenberger, D. L.; El-khateeb, M.; Weigand, W. *Organometallics* **2009**, *28*, 1039–1048.
(13) Liu, T.; Li, B.; Singleton, M. L.; Hall, M. B.; Darensbourg, M. Y. *J. Am. Chem. Soc.* **2009**, *131*, 8296–8307.
(14) Lyon, E. J.; Georgakaki, I. P.; Reibenspies, J. H.; Darensbourg, M. Y. *Angew. Chem., Int. Ed.* **1999**, *38*, 3178–3180.
(15) Schmidt, M.; Contakes, S. M.; Rauchfuss, T. B. *J. Am. Chem. Soc.* **1999**, *121*, 9736–9737.
(16) Gloaguen, F.; Lawrence, J. D.; Schmidt, M.; Wilson, S. R.; Rauchfuss, T. B. *J. Am. Chem. Soc.* **2001**, *123*, 12518–12527.
(17) Li, P.; Wang, M.; He, C.-J.; Liu, X.-Y.; Jin, K.; Sun, L.-C. *Eur. J. Inorg. Chem.* **2007**, *2007*, 3718–3727.

Chart 1. [a]

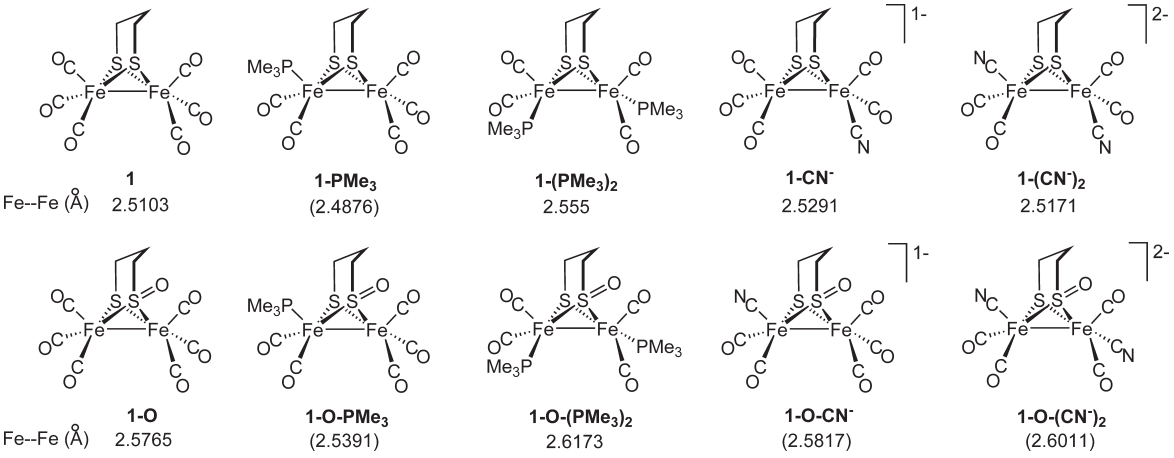

[a] Experimental or (DFT Calculated) Fe−Fe distances underneath each structure.

stirred for 0.5 h. The solvent was removed under vacuum, and the dark red residue was recrystallized from 5 mL of CH_2Cl_2 by gradual addition of 30 mL of Et_2O. The resulting red solid was washed with 3 × 20 mL of Et_2O and dried under vacuum. Yield: 387 mg (73%). ^{1}H NMR (DMSO-d_6, 300 MHz): δ = 3.18 (m, 8H, N(CH_2CH$_3$)$_4$), 2.07 (br, 2H, O=SCH_2), 1.92 (br, 2H, SCH_2), 1.63 (br, 2H, CH$_2$CH_2CH$_2$), 1.15 (m, 12H, N(CH$_2$-CH_3)$_4$). IR (CH$_3$CN, cm^{-1}): ν (CN) = 2099(w); ν (CO) = 2042(m), 1993(s), 1975(s), 1958(m), 1934(m). ESI-MS (CH_2Cl_2, m/z): 399.9, [M − Et_4N^+]; 371.9, [M − Et_4N^+ − CO]; 343.9, [M − Et_4N^+ − 2CO]; 315.9, [M − Et_4N^+ − 3CO].

[Et$_4$N]$_2${(μ-pst)[Fe(CO)$_2$CN]$_2$} (1-O-(CN)$_2^{2-}$). To a solution of compound **1-O** (80 mg, 0.2 mmol) in 10 mL of CH_3CN was added $Et_4N^+CN^-$ (188 mg, 1.2 mmol) dissolved in 10 mL of CH_3CN; the reaction mixture was heated to reflux and stirred overnight. The excess $Et_4N^+CN^-$ was removed by precipitation on gradual addition of Et_2O. After filtration the filtrate was dried under vacuum. The crude product was purified by recrystallization from 5 mL of CH_2Cl_2 layered with Et_2O. Yield, ~70%. ^{1}H NMR (DMSO-d_6, 300 MHz): δ = 3.20 (m, 16H, N(CH_2CH$_3$)$_4$), 1.93 (br, 2H, O=SCH_2), 1.75 (m, 2H, SCH_2), 1.64 (br, 2H, CH$_2$CH_2CH$_2$), 1.15 (m, 24H, N(CH$_2$CH_3)$_4$). IR (CH$_3$CN, cm^{-1}): ν (CN) = 2075(m); ν (CO) = 1979(s), 1939(s), 1903(s).

Kinetic Measurements. Pseudo-first-order reaction conditions were employed for all kinetic studies, using 20-fold and greater excesses of PMe_3 or $Et_4N^+CN^-$. Reactions were monitored by infrared spectroscopy. Typically, 10 mL of a toluene (or CH_3CN for the $Et_4N^+CN^-$ substitution) solution containing the diiron complex (0.10 mmolar) in a Schlenk flask under N_2 was placed in a temperature-controlled bath. Following temperature equilibration, 10 mL of a toluene solution of PMe_3 (or an CH_3CN solution of $Et_4N^+CN^-$) at the same temperature was rapidly transferred into the flask. While being magnetically stirred, samples were removed, and IR spectra were taken at 2 to 40 min intervals typically through four half-lives. Rates of reaction were measured by following the decrease in absorption of the reactant's most intense non-overlapping ν(CO) vibration, which centered at about 2073 cm^{-1} for complex **1**; 2036 cm^{-1} for **1-PMe$_3$**; 2083 cm^{-1} for complex **1-O**; and 2042 cm^{-1} for **1-O-CN$^-$**. Rate constants were calculated from plots of ln(A_0/A_t) versus time typically using > 30 data points over 4 to 5 half-lives giving correlation constant of 0.99. Reproducibility of a run under indentical conditions was 95% or better. Activation parameters $\Delta H^{\ddagger}$, $\Delta S^{\ddagger}$ were obtained from Eyring plots; activation energies, E_a, were obtained from Arrhenius plots.

Theoretical Details. DFT calculations were performed using a hybrid functional [the three parameter exchange functional of Becke (B3)[18] and the correlation functional of Lee, Yang, and Parr (LYP) (B3LYP) as implemented in Gaussian 03].[19,20] The effective core potentials and associated basis set of Hay and Wadt (LANL2DZ)[21,22] were used on the iron and sulfur atoms. For iron, the two outermost p functions were replaced by the reoptimized 4p functions as suggested by Couty and Hall.[23] For sulfur, the basis set was augmented by the d polarization function of Höllwarth et al.[24] All carbon, oxygen, and hydrogen atoms were represented using Dunning's double-ζ valence basis set (D95).[25,26] The geometries of all oxygenate isomers and corresponding transition states were fully optimized and confirmed as minima or first-order saddle points by analytical frequency calculations at the same levels.

Results and Discussion

Properties of Complexes 1, 1-O, and CN$^-$/PMe$_3$ Substituted Derivatives. With the exception of **1-O-CN$^-$** and **1-O-(CN)$_2^{2-}$**, all complexes in this study, Chart 1, are from literature preparations. The sulfenato-monocyanide complex was readily obtained (30 min to completion)

(18) Becke, A. D. *J. Chem. Phys.* **1993**, *98*, 5648–5652.
(19) Lee, C.; Yang, W.; Parr, R. G. *Phys. Rev. B: Condens. Matter* **1988**, *37*, 785.
(20) Frisch, M. J.; Trucks, G. W.; Schlegel, H. B.; Scuseria, G. E.; Robb, M.; Cheeseman, J. R.; Montgomery, J. A.; Vreven, J. A.; Kudin, K. N.; Burant, J. C.; Millam, J. M.; Iyengar, S. S.; Tomasi, J.; Barone, V.; Mennucci, B.; Cossi, M.; Scalmani, G.; Rega, N.; Petersson, G. A.; Nakatsuji, H.; Hada, M.; Ehara, M.; Toyota, K.; Fukuda, R.; Hasegawa, J.; Ishida, M.; Nakajima, T.; Honda, Y.; Kitao, O.; Nakai, H.; Klene, M.; Li, X.; Knox, J. E.; Hratchian, H. P.; Cross, J. B.; Adamo, C.; Jaramillo, J; Gomperts, R.; Stratmann, R. E.; Yazyev, O.; Austin, A. J.; Cammi, R.; Pomelli, C.; Ochterski, J. W.; Ayala, P. Y.; Morokuma, K.; Voth, G. A.; Salvador, P.; Dannenberg, J. J.; Zakrzewski, V. G.; Dapprich, S.; Daniels, A. D.; Strain, M. C.; Farkas, O.; Malick, D. K.; Rabuck, A. D.; Raghavachari, K.; Foresman, J. B.; Ortiz, J. V.; Cui, Q.; Baboul, A. G.; Clifford, S.; Cioslowski, J.; Stefanov, B. B.; Liu, G.; Liashenko, A.; Piskorz, P.; Komaromi, I.; Martin, R. L.; Fox, D. J.; Keith, T.; Al-Laham, M. A.; Peng, C. Y.; Nanayakkara, A.; Challacombe, M.; Gill, P. M. W.; Johnson, B.; Chen, W.; Wong, M. W.; Gonzalez, C.; Pople, G. A. *Gaussian 03*, Revision B.04; Gaussian, Inc.: Wallingford, CT, 2004.
(21) Hay, P. J.; Wadt, W. R. *J. Chem. Phys.* **1985**, *82*, 270–283.
(22) Wadt, W. R.; Hay, P. J. *J. Chem. Phys.* **1985**, *82*, 284–298.
(23) Marc Couty, M. B. H. *J. Comput. Chem.* **1996**, *17*, 1359–1370.
(24) Höllwarth, A.; Böhme, M.; Dapprich, S.; Ehlers, A. W.; Gobbi, A.; Jonas, V.; Köhler, K. F.; Stegmann, R.; Veldkamp, A.; Frenking, G. *Chem. Phys. Lett.* **1993**, *208*, 237–240.
(25) Dunning, J. T. H. *J. Chem. Phys.* **1970**, *53*, 2823–2833.
(26) Dunning, T. H., Jr.; Hay, P. J. In *Methods of Electronic Structure Theory*; Schaefer, H. F., III, Ed.; Plenum Press: New York, 1977; p 3.

Table 1. Infrared Spectroscopic (ν(CO) and ν(**CN**)) Data For (μ-pdt)[Fe(CO)$_2$(L)]$_2$ and (μ-pst)[Fe(CO)$_2$(L)]$_2$ Derivatives[a]

compound	ν (**CN**), ν(CO) (cm^{-1})
(μ-pdt)[Fe(CO)$_3$]$_2$ (**1**)	2072(m), 2032(s), 2000(m), 1987(m)
(μ-pst)[Fe(CO)$_3$]$_2$ (**1-O**)	2081(m), 2042(s), 2017(m), 1995(m)
(μ-pdt)[Fe(CO)$_3$][Fe(CO)$_2$PMe$_3$] (**1-PMe$_3$**)	2036(m), 1981(s), 1960(m), 1923(m)
(μ-pst)[Fe(CO)$_3$][Fe(CO)$_2$PMe$_3$][c] (**1-O-PMe$_3$**)	2049(m), 1992(s), 1973(m), 1934(m)
(μ-pdt)[Fe(CO)$_2$PMe$_3$]$_2$ (**1-(PMe$_3$)$_2$**)	1982(w), 1944(s), 1902(s)
(μ-pst)[Fe(CO)$_2$PMe$_3$]$_2$ (**1-O-(PMe$_3$)$_2$**)	1983(w), 1956(s), 1919(m), 1906(m)
(μ-pdt)[Fe(CO)$_3$][Fe(CO)$_2$CN$^-$][b] (**1-CN$^-$**)	**2094**(w); 2029(s), 1974(s), 1955(s), 1941(vs), 1917(s br)
(μ-pst)[Fe(CO)$_3$][Fe(CO)$_2$CN$^-$][c] (**1-O-CN$^-$**)	**2099**(w); 2042(m), 1993(s), 1975(s), 1958(m), 1934(m)
(μ-pdt)[Fe(CO)$_2$CN$^-$]$_2$ [c] (**1-(CN)$_2^{2-}$**)	**2076** (w), **2032** (w); 1964 (s), 1923 (s), 1883 (s)
(μ-pst)[Fe(CO)$_2$CN$^-$]$_2$ [c] (**1-O-(CN)$_2^{2-}$**)	**2075**(m); 1979(s), 1939(s), 1903(s)

[a] Reported in toluene solution unless otherwise noted. [b] Spectra recorded in THF. [c] Spectra recorded in acetonitrile; Et_4N^+ counterion.

from CO/CN$^-$ (as its Et_4N^+ salt) exchange into **1-O** at 60 °C, while excess CN$^-$ at CH$_3$CN reflux overnight was required to obtain **1-O-(CN)$_2^{2-}$**, eq 1. Note that these conditions are much harsher than those used for similar CN$^-$ incorporation into complex **1** where only the dicyanide **1-(CN)$_2^{2-}$** was observed even at substoichiometric amounts of CN$^-$ and at −8 °C.[1] Our efforts to obtain the extremely air-sensitive **1-O**-cyano complexes in pure crystalline form were unsuccessful.

$$\textbf{1-O} \xrightarrow[60°C,\ 0.5h]{CN^-,\ CH_3CN} [\textbf{1-O-CN}]^- \xrightarrow[>80°C,\ 12h]{xsCN^-,\ CH_3CN} [\textbf{1-O-(CN)}_2]^{2-} \quad (1)$$

The structures of reactants and products in this study are largely known, Chart 1. In the case of the calculated structures shown in Chart 1, differences in apical/basal isomers may be as large as 4 kcal/mol, while isomeric forms derived from the chair/boat configuration possibilities of the pseudocyclohexane FeS_2C_3 ring are on the order of 2 kcal/mol.[13]

Table 1 contains the ν(CO) and ν(CN) infrared spectral data for the complexes of Chart 1. Notably, complexes based on complex **1** versus **1-O** of analogous composition display similar IR patterns; however, ν(CO) values of the (μ-pst)[Fe(CO)$_2$L]$_2$ thiolate/sulfenate bridged compounds shift to higher energies by 10 to 20 cm^{-1} as compared to the dithiolate (μ-pdt)[Fe(CO)$_2$L]$_2$ derivatives. This reflects the poorer electron donating ability of the sulfenato sulfur and a decrease of electron density at the [FeFe] unit as compared to the dithiolate bridge ligand in the μ-pdt complexes.

Kinetic Studies of PMe$_3$/CO Substitution in (μ-pdt)[Fe(CO)$_3$]$_2$ (1). Reactions of complex **1** with PMe$_3$ to yield **1-PMe$_3$**, eq 2, were carried out in toluene solution, under pseudo-first-order conditions of 20-fold and greater excesses of PMe$_3$. Figure 2a presents stacked plots of

$$\textbf{1} + \text{xsPMe}_3 \xrightarrow{\text{Toluene}} \textbf{1-PMe}_3 \quad (2)$$

$$\text{Rate} = k_{obs}[\textbf{1}] = k_2[\textbf{1}][\text{PMe}_3] \quad (3)$$

infrared spectra in the 2000 cm^{-1} region which illustrate the rate data obtained for this reaction; in the example, spectra were recorded at 2 min intervals. Kinetic parameters for the reactions of complex **1** with PMe$_3$ were determined by monitoring the disappearance of the ν(CO)

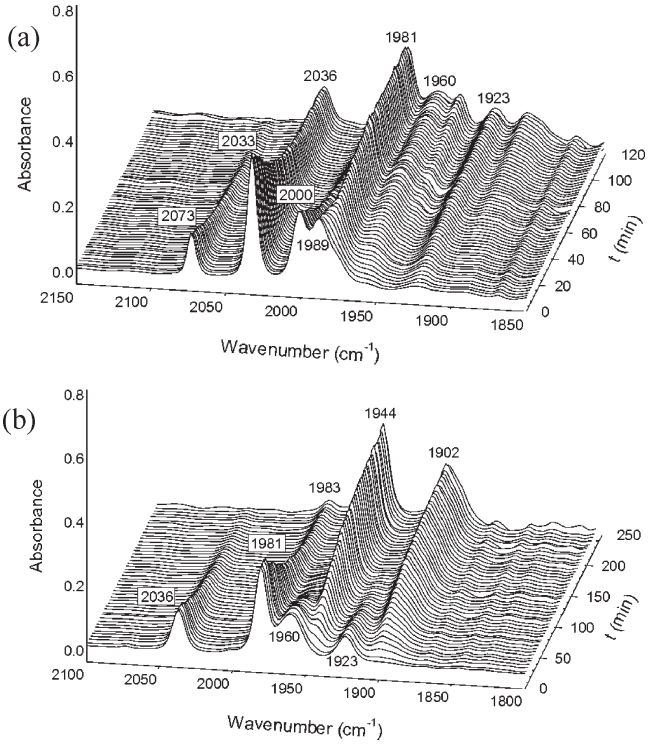

Figure 2. Infrared spectra, in the 1800−2150 cm^{-1} region, as CO/PMe$_3$ exchange takes place to produce (a) **1-PMe$_3$** from **1**; and (b) to produce **1-(PMe$_3$)$_2$** from **1-PMe$_3$**.

band at 2073 cm^{-1} with time. The disappearance of the ν(CO) band at 2000 cm^{-1} yielded similar results. The data measured at 22 °C were used to determine the rate expression; plots of $\ln(A_0/A_t)$ versus time showed good linearity over 5 half-lives, Figure 3a. The derived values of k_{obs} at various PMe$_3$ concentrations are given in Table 2, entries 1−4. Each k_{obs} was obtained from a single kinetic run, with ~30 spectral accumulations per run. The plot of k_{obs} versus [PMe$_3$] shows good linearity, Figure 3b, and its zero intercept indicates that the reaction described in eq 2 follows a second-order rate expression, eq 3.

Under similar conditions, sample stacked plots for the reaction of **1-PMe$_3$** with PMe$_3$ in toluene solution at 50 °C, eq 4, are shown in Figure 2b. The disappearance of the band at 2036 cm^{-1} showed linearity in the $\ln(A_0/A_t)$ versus time plot, as well as a first-order dependence on [PMe$_3$], eq 5. The rate constants k_2 derived from these data measured at 50 °C, entries 5−8 in Table 2, are smaller than those obtained from the first-step, (μ-pdt)-[Fe(CO)$_3$]$_2$/PMe$_3$ substitution reaction measured at

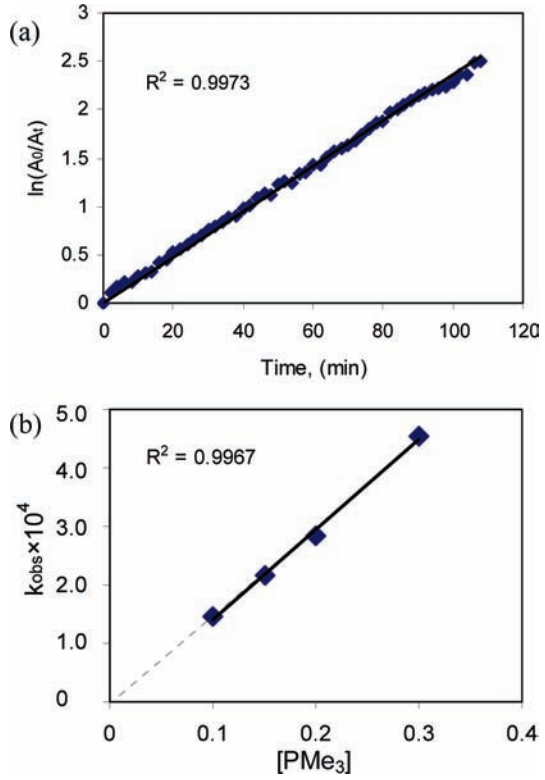

Figure 3. (a) Example of plot of $\ln(A_0/A_t)$ vs time over five half-lives, Entry 4, Table 2. (b) Plot of k_{obs} vs $[PMe_3]$ for the formation of complex **1-PMe$_3$** from complex **1** measured at 22 °C.

Table 2. Rate Data for Determination of Rate Expression for the Reaction of PMe_3 with Complex **1** Measured at 22 °C and with **1-PMe$_3$** Measured at 50 °C in Toluene Solution

entry	rxn	$[PMe_3]$, M	$10^4\ k_{obs}$, sec^{-1}
1	**1** → **1-PMe$_3$** [a]	0.10	1.47
2	**1** → **1-PMe$_3$**	0.15	2.15
3	**1** → **1-PMe$_3$**	0.20	2.85
4	**1** → **1-PMe$_3$**	0.30	4.55
	av k_2 = 14.6 (±0.6) × 10^{-4} M^{-1} sec^{-1}		
5	**1-PMe$_3$** → **1-(PMe$_3$)$_2$** [a]	0.10	1.28
6	**1-PMe$_3$** → **1-(PMe$_3$)$_2$**	0.15	1.97
7	**1-PMe$_3$** → **1-(PMe$_3$)$_2$**	0.20	2.62
8	**1-PMe$_3$** → **1-(PMe$_3$)$_2$**	0.30	4.00
	av k_2' = 13.1 (±0.3) × 10^{-4} M^{-1} sec^{-1}		

[a] $[Fe_2] = 5.0 \times 10^{-3}$ M with 20−60-fold excess PMe_3.

22 °C, entries 1−4.

$$\textbf{1-PMe}_3 + \text{xsPMe}_3 \xrightarrow{\text{Toluene}} \textbf{1-(PMe}_3)_2 \qquad (4)$$

$$\text{Rate} = k_{obs}'[\textbf{1-PMe}_3] = k_2'[\textbf{1-PMe}_3][PMe_3] \qquad (5)$$

Kinetic Studies of PMe_3/CO Exchange into (μ-pst)[Fe(CO)$_3$]$_2$ (1-O). Reactions of (μ-pst)[Fe(CO)$_3$]$_2$ (**1-O**) with PMe_3 to yield (μ-pst)[Fe(CO)$_3$][Fe(CO)$_2$PMe$_3$] (**1-O-PMe$_3$**), eq 6, were carried out in toluene solution at 80, 90, 95, and 100 °C, under pseudo-first-order conditions of 20-fold and greater excesses of PMe_3. Kinetic parameters for the reactions of **1-O** with PMe_3 were determined by monitoring the disappearance of the ν(CO) band at 2081 cm^{-1} with time, augmented by the disappearance of the ν(CO) band at 2017 cm^{-1}, Figure 4. The plots of $\ln(A_0/A_t)$ versus time showed good linearity; Figure 5a. The derived values of k_{obs} at various PMe_3 concentrations and reaction temperatures, as determined by infrared spectroscopy, are given in Table 3, entries 1−12. Each k_{obs} was obtained from a single kinetic run, with at least ~12 spectral accumulations per run. The plot of k_{obs} versus $[PMe_3]$, Figure 5b (90 °C), shows linearity; however, a nonzero intercept indicates the reaction does not follow a strict second-order rate expression, but rather both associative (A) and dissociative (D) substitution processes are assumed to be involved at the higher reaction temperatures, eq 7. Hence, the plot of k_{obs} versus $[PMe_3]$, Figure 5b and eq 8, yields the dissociative substitution rate constant, $k_1 = 1.92 \times 10^{-5}$ sec^{-1}, derived from the intercept and the associative substitution rate constant, $k_2 = 1.58 \times 10^{-4}$ M^{-1} sec^{-1}, is determined from the slope. It should be noted that the IR traces appeared to represent a quantitative reaction and reproducibility at 95 °C is on the order of 95%. However, some decomposition

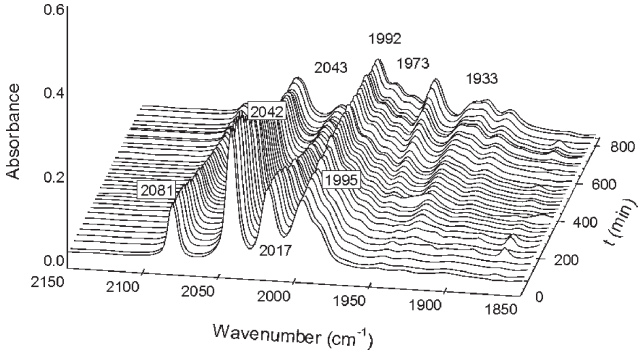

Figure 4. Infrared spectra, in the 1800−2150 cm^{-1} region, as CO/PMe_3 exchange takes place to produce complex **1-O-PMe$_3$** from **1-O**.

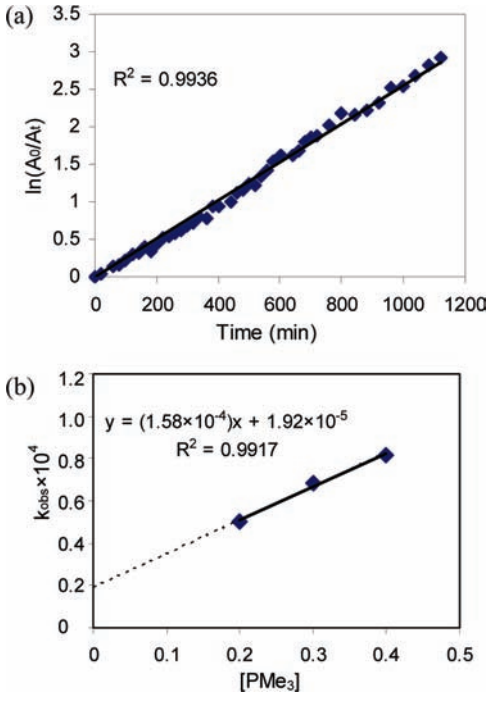

Figure 5. (a) Example of plot of $\ln(A_0/A_t)$ vs time over four half-lives, Entry 7, Table 3. (b) Plots of k_{obs} vs $[PMe_3]$ for the formation of **1-O-PMe$_3$** from **1-O** measured at 90 °C.

Table 3. Rate Data for the Reaction of PMe_3 with (μ-pst)[$Fe(CO)_3$]$_2$ (**1-O**) as a Function of Temperature in Toluene[a]

entry	temp., °C	[PMe_3], M	$10^4\,k_{obs}$, sec^{-1}
1	80	0.20	0.28
2	80	0.30	0.33
3	80	0.40	0.45
4	90	0.20	0.50
5	90	0.30	0.68
6	90	0.40	0.82
7	95	0.20	0.80
8	95	0.30	0.90
9	95	0.40	1.18
10	100	0.20	1.23
11	100	0.30	1.58
12	100	0.40	1.73

[a] $[Fe_2] = 5.0 \times 10^{-3}$ M with 40−80-fold excess PMe_3.

Table 4. Temperature Dependence of Reaction of PMe_3 with (μ-pdt)[$Fe(CO)_3$]$_2$ (**1**), (μ-pdt)[$Fe(CO)_3$][$Fe(CO)_2PMe_3$] (**1-PMe$_3$**), and (μ-pst)[$Fe(CO)_3$]$_2$ (**1-O**)

Rxn path	T,°C	k	activation parameters[c]
1 → **1-PMe$_3$** [a]		$10^3\,k_2$, $M^{-1}\,s^{-1}$	
	22	1.47	E_a = 48 kJ/mol
	30	2.55	$\Delta H^{\ddagger}$ = 45 (±1) kJ/mol
	40	4.50	$\Delta S^{\ddagger}$ = −145 (±3) J/mol K
	50	8.08	
1-PMe$_3$ → **1-(PMe$_3$)$_2$** [a]		$10^3\,k_2'$, $M^{-1}\,s^{-1}$	
	50	1.28	E_a = 53 kJ/mol
	60	2.67	$\Delta H^{\ddagger}$ = 50 (±4) kJ/mol
	70	4.48	$\Delta S^{\ddagger}$ = −146(±11) J/mol K
	80	6.87	
1-O → **1-O-PMe$_3$** [b] (A path)		$10^4\,k_2$, $M^{-1}\,s^{-1}$	
	80	0.83	E_a = 60 kJ/mol
	90	1.58	$\Delta H^{\ddagger}$ = 56 (±3) kJ/mol
	95	1.92	$\Delta S^{\ddagger}$ = −163(±9) J/mol K
	100	2.50	
1-O → **1-O-PMe$_3$** [b] (D path)		$10^5\,k_1$, s^{-1}	
	80	1.06	E_a = 107 kJ/mol
	90	1.92	$\Delta H^{\ddagger}$ = 104(±18) kJ/mol
	95	3.86	$\Delta S^{\ddagger}$ = −50 (±49) J/mol K
	100	7.67	

[a] $[Fe_2] = 5.0 \times 10^{-3}$ M; [PMe_3] = 0.1 M. [b] $[Fe_2] = 5.0 \times 10^{-3}$ M; [PMe_3] = 0.2−0.4 M. [c] Errors in activation parameters reported at 95% confidence level.

cannot be ruled out.

$$\textbf{1-O} + \text{xs } PMe_3 \xrightarrow{\text{Toluene}} \textbf{1-O-PMe}_3 \qquad (6)$$

$$\text{Rate} = k_1[\textbf{1-O}] + k_2[\textbf{1-O}][PMe_3] \qquad (7)$$

$$\text{Rate} = k_{obs}[\textbf{1-O}]; \quad k_{obs} = k_1 + k_2[PMe_3] \qquad (8)$$

The reaction of **1-O-PMe$_3$** with PMe_3 to yield **1-O-(PMe$_3$)$_2$** is extremely slow under similar conditions as above, and kinetic measurements were not conducted.

Temperature Dependence of Reactions of Complexes 1, 1-PMe$_3$, and 1-O with PMe$_3$. The temperature-dependence of rate constants for the formation of complex **1-PMe$_3$** starting from complex **1** and the formation of complex **1-(PMe$_3$)$_2$** starting from complex **1-PMe$_3$** are given in Table 4. Table 4 lists values for the enthalpy and entropy of activation derived from Eyring plots, Figure 6, as well as E_{act} derived from Arrhenius plots, Supporting Information, Figure S1. Consistent with the second-order rate expressions for the respective associative or I_a mechanisms, $\Delta H^{\ddagger}$ values are small to moderate and $\Delta S^{\ddagger}$ values are large and negative. The similar values of $\Delta S^{\ddagger}$ and increased values of $\Delta H^{\ddagger}$ and E_{act} of the reactions described by eqs 2 and 4, suggest the addition of the second PMe_3 is the overall rate-limiting step in the production of complex **1-(PMe$_3$)$_2$** starting from **1**.

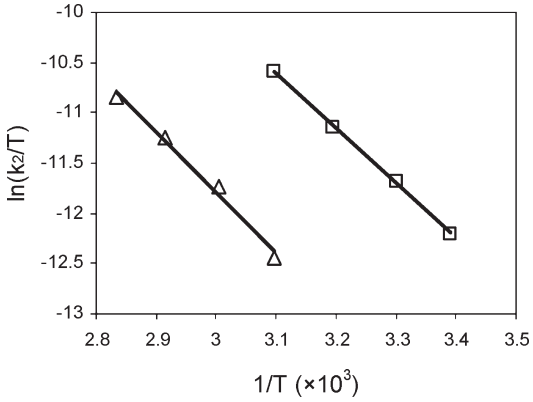

Figure 6. Eyring plots for the formation of complex **1-PMe$_3$** from complex **1** (□) and for the formation of **1-(PMe$_3$)$_2$** from **1-PMe$_3$** (Δ).

The temperature dependence of rate constants for both the D and A pathways for formation of complex **1-O-PMe$_3$** from **1-O** are also given in Table 4 and presented graphically as Eyring and Arrhenius plots, Supporting Information, Figure S2; the calculated values for the enthalpy and entropy of activation as well as the E_{act} derived from Arrhenius plots are listed. The small values of $\Delta H^{\ddagger}$ and large negative values for $\Delta S^{\ddagger}$ are consistent with the associative pathway. For the dissociative pathway, $\Delta H^{\ddagger}$ and E_{act} values of about 100 kJ/mol are as expected for dissociation of the CO ligand in the rate-determining step.

Kinetic Studies of CN^-/CO Exchange into (μ-pst)[Fe(CO)$_3$]$_2$ (1-O). The reaction of complex **1-O** with $Et_4N^+CN^-$ carried out in CH_3CN solution at 0 °C under pseudo-first-order conditions of a 20-fold excess of $Et_4N^+CN^-$ was found to produce only the monosubstituted [Et_4N]{(μ-pst)[$Fe(CO)_3$][$Fe(CO)_2CN$]} (**1-O-CN$^-$**), eq 9. The rapid disappearance of the band at 2083 cm^{-1}, Figure 7a, allowed only 14 data points for the determination of ln Abs versus T and the k_2 value, given as entry 1 in Table 5. The large k_2 values indicated the ease of attack of complex **1-O** by CN^-. A second study performed at a 10-fold excess of CN^- yielded a k_2 value roughly 1/2 that of the 20-fold excess; hence, we suggest the rate expression of eq 10 holds as well for this reaction.

$$\textbf{1-O} + \text{xs}Et_4NCN \xrightarrow{CH_3CN} \textbf{1-O-CN}^- \qquad (9)$$

$$\text{Rate} = k_{obs}[\textbf{1-O}] = k_2[\textbf{1-O}][\textbf{CN}^-] \qquad (10)$$

The mono-cyanide-substituted complex **1-O-CN$^-$**, produced *in situ* at low temperature, was used in subsequent kinetic studies of the addition of the second CN^-, eq 11.

$$\textbf{1-O-CN}^- + \text{xs}Et_4NCN \xrightarrow{CH_3CN} (\textbf{1-O-CN}_\textbf{2})^{2-} \qquad (11)$$

$$\text{Rate} = k_{obs}'[\textbf{1-O-CN}^-] = k_2'[\textbf{1-O-CN}^-][\textbf{CN}^-] \qquad (12)$$

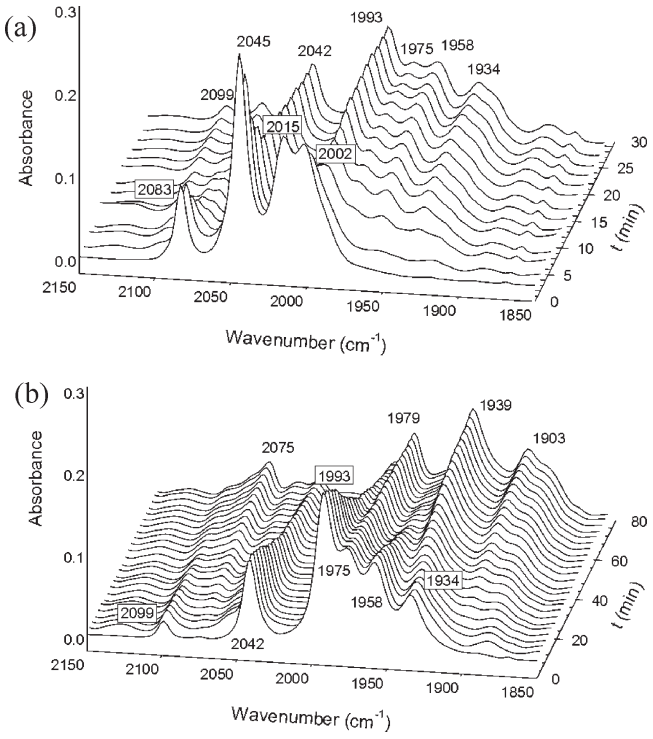

Figure 7. Infrared spectra, in the 1850−2150 cm^{-1} region, as CO/CN^- exchange takes place (a) to produce **1-O-CN**$^-$ from **1-O** at 0 °C in CH_3CN, and (b) to produce $(\mathbf{1\text{-}O\text{-}CN_2})^{2-}$ from **1-O-CN**$^-$ at 40 °C in CH_3CN.

Table 5. Rate Data for the Reaction of $Et_4N^+CN^-$ with Complex **1-O** Measured at 0 °C and with **1-O-CN**$^-$ Measured at 40 °C in CH_3CN Solution

entry	rxn	$[CN^-]$, M	$10^4\ k_{obs}$, sec^{-1}
1	**1-O** → **1-O-CN**$^-$ [a]	0.05	6.57
2	**1-O** → **1-O-CN**$^-$	0.10	14.6
	av k_2 = 138.8 (±7.4) × 10^{-4} M^{-1} sec^{-1}		
3	**1-O-CN**$^-$ → **1-O-(CN)**$_2^{2-}$ [b]	0.10	0.83
4	**1-O-CN**$^-$ → **1-O-(CN)**$_2^{2-}$	0.15	1.08
5	**1-O-CN**$^-$ → **1-O-(CN)**$_2^{2-}$	0.20	1.62
6	**1-O-CN**$^-$ → **1-O-(CN)**$_2^{2-}$	0.30	2.43
	av k_2' = 7.94 (±0.8) × 10^{-4} M^{-1} sec^{-1}		

[a] $[Fe_2]$ = 5.0 × 10^{-3} M with 10−20-fold excess CN^-; 0 °C. [b] $[Fe_2]$ = 5.0 × 10^{-3} M with 20−60-fold excess CN^-; 40 °C.

Figure 7b presents stacked plots of ν(CO) IR spectra for the reaction of **1-O-CN**$^-$ with CN^- taken at 3 min intervals. By monitoring the disappearance of the ν(CO) band at 2042 cm^{-1} with time, the data measured at 40 °C were used to determine the rate expression. Plots of $\ln(A_0/A_t)$ versus time showed good linearity over 4 half-lives, Figure 8a. The derived values of k_{obs} at various $Et_4N^+CN^-$ concentrations, entries 2−5 measured at 40 °C in Table 5, are much smaller than that obtained from the first-step (μ-pst)$[Fe(CO)_3]_2/CN^-$ reaction measured at 0 °C. The plot of k_{obs} versus $[CN^-]$ shows good linearity, Figure 8b, the zero intercept indicates the rate determining step for the overall reaction follows a second-order rate expression, eq 12.

Temperature Dependence of Reactions of Complex 1-O-CN$^-$ **with Et$_4$N$^+$CN$^-$.** Table 6 lists values for the enthalpy and entropy of activation for the formation of complex $(\mathbf{1\text{-}O\text{-}CN_2})^{2-}$ starting from complex **1-O-CN**$^-$ derived from Eyring plots, Figure 9, as well as E_{act} derived from Arrhenius plots, Supporting Information, Figure S3. As described above for the PMe_3 associative reactivity, $\Delta H^{\ddagger}$ values are small to moderate and $\Delta S^{\ddagger}$ values are large and negative.

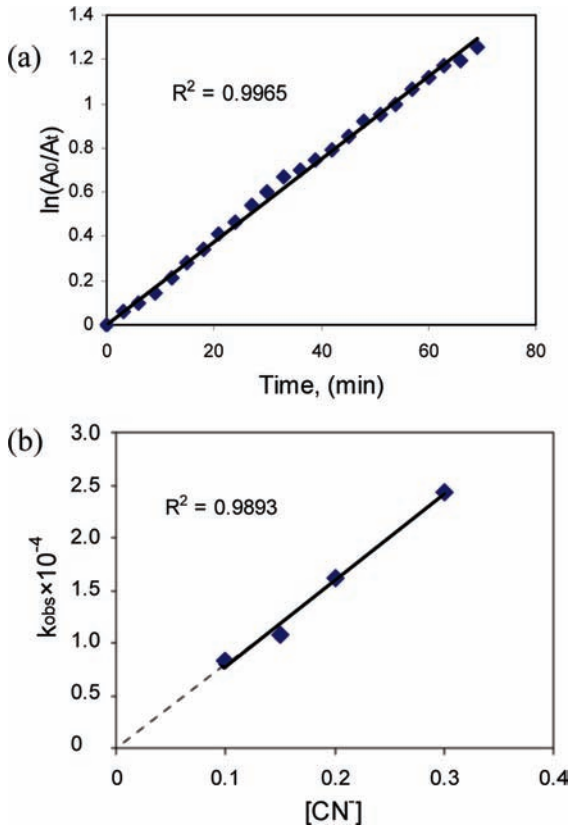

Figure 8. (a) Example of plot of $\ln(A_0/A_t)$ vs time over three half-lives. (b) Plot of k_{obs} vs $[CN^-]$ for the formation of $(\mathbf{1\text{-}O\text{-}CN_2})^{2-}$ from **1-O-CN**$^-$ measured at 40 °C.

The monitor of CN^-/CO substitution into complex (μ-pst)$[Fe(CO)_3]_2$ (**1-O**) shows faster rates and lower E_{act} barriers to the first and second CN^- ligand additions as compared to the PMe_3 exchange into complex **1-O** but is otherwise kinetically and mechanistically analogous. The formation of **1-O-CN**$^-$ was observed clearly to be an intermediate step for the overall ligand exchange reaction to produce **1-O-(CN)**$_2^{2-}$. The harsher reaction conditions and large activation parameters of CN^-/CO exchange into **1-O-CN**$^-$ indicate the second substitution to be rate-limiting, with the association of the CN^- and the diiron complex following a similar pathway as found for the PMe_3 reactions. This relative ordering of the first and second step is different from the CN^-/CO exchange into complex **1**. Values of E_a (61 kJ/mol), $\Delta H^{\ddagger}$ (58 kJ/mol) of the CN^-/CO exchange into **1-O-CN**$^-$ to form **1-O-(CN)**$_2^{2-}$ are almost twice larger than the E_a (36 kJ/mol) and $\Delta H^{\ddagger}$ (34 kJ/mol) of the CN^-/CO exchange into **1-CN**$^-$ to form **1-(CN)**$_2^{2-}$.[1] Thus, the activation energy barrier for CN^-/CO exchange in **1-O-CN**$^-$ has been increased by the presence and effect of the sulfenato-oxygen. *As the electrophilicity of the iron centers in the **1-O** derivatives should increase relative to **1**, we look to the fluxionality of the diiron complex for explanation of this switch in reactivity*

Intramolecular CO Site-Exchange Processes of Complex 1-O-CN$^-$ **via Variable Temperature ^{13}C NMR Studies.** In a recent study we showed that the intramolecular exchange of

Table 6. Temperature Dependence of Reaction of $Et_4N^+CN^-$ with Complex (**1-O-CN**$^-$): **1-O-CN**$^-$ → **1-O-(CN)**$_2^{2-a}$

T, °C	(10^3) k_2, M^{-1} s^{-1}	activation parameters[b]
40	0.83	E_a = 61 kJ/mol
50	1.63	$\Delta H^{\ddagger}$ = 58 (±2) kJ/mol
60	3.12	$\Delta S^{\ddagger}$ = −119 (±7) J/mol K
70	6.55	

[a] $[Fe_2] = 5.0 \times 10^{-3}$ M; $[CN^-] = 0.1$ M. [b] Errors in activation parameters reported at 95% confidence level.

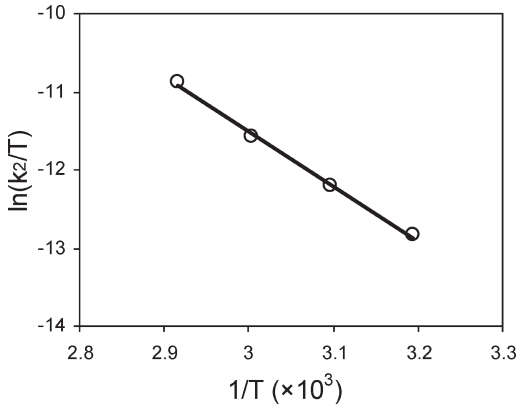

Figure 9. Eyring plot for the formation of complex **1-O-(CN)**$_2^{2-}$ from complex **1-O-CN**$^-$

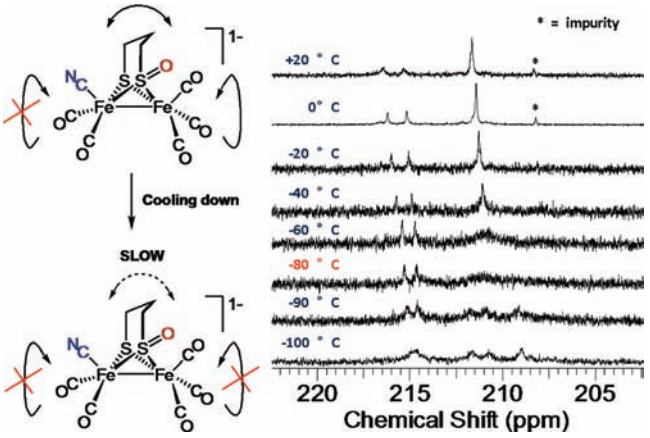

Figure 10. Variable temperature ^{13}C NMR studies of complex **1-O-CN**$^-$ from −100 to 20 °C (CD_2Cl_2 solution, in CO region); signal indicated with a "*" symbol are impurities.

CO groups in **1-O** had a larger barrier for the $Fe(CO)_3$ rotor process than that found for complex **1**.[13] Here we explore the effect of Fe-bound CN^- on the CO-site exchange in **1-O-CN**$^-$. Figure 10 displays ^{13}C NMR spectra in the CO region of the **1-O-CN**$^-$ complex over the temperature range of −100 to 20 °C. At −100 °C, three separate resonances are seen at 209.0, 210.8, and 211.6 ppm, which on warming are found to coalesce by −80 °C, reforming into a single sharp resonance at −40 °C and above. This resonance is assigned to the carbons of the $Fe(CO)_3$ unit which are in rapid intramolecular exchange at 20 °C. In contrast, the two resonances at 215.2 and 216.2 at 20 °C, assigned to the carbonyl carbons of the $Fe(CO)_2(CN)$ unit, remain distinct on cooling to −90 °C, but display a gradual broadening that gives rise to an apparent broad signal at 214.8 ppm at

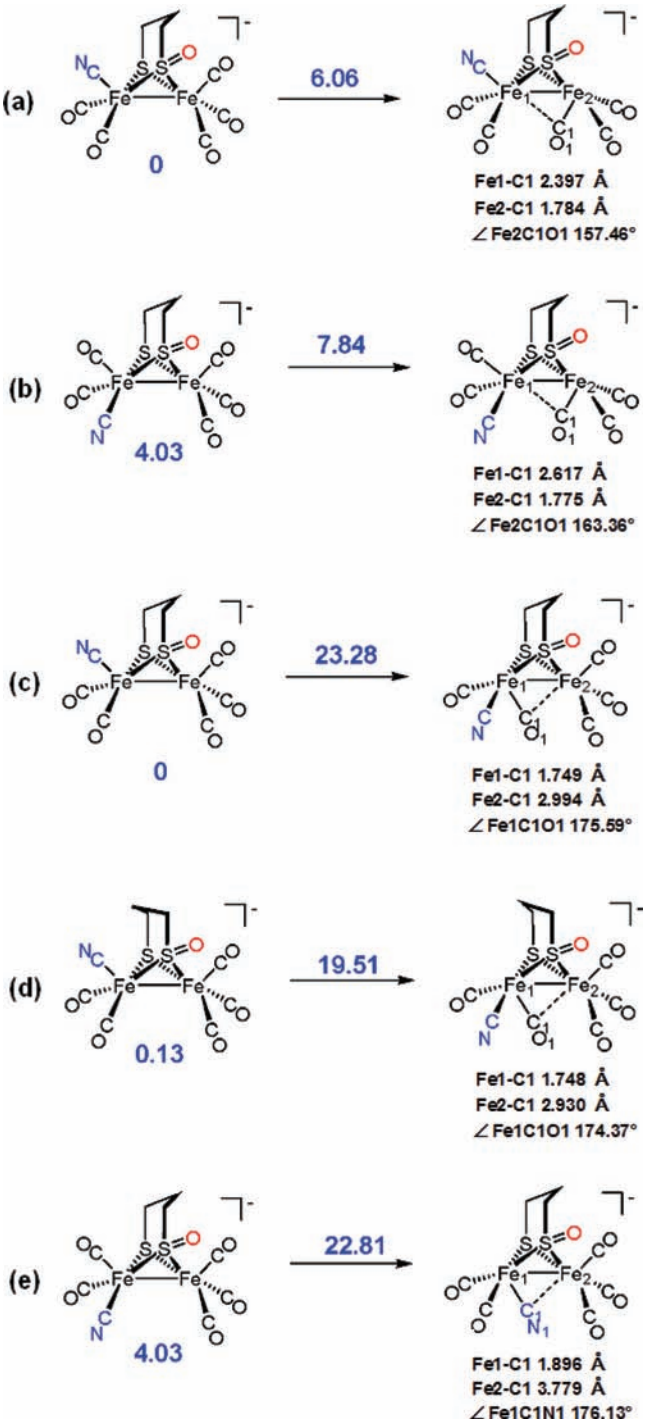

Figure 11. Ground state and transition state structures for the rotation of $Fe(CO)_3$ and $Fe(CO)_2CN^-$ units in the complex **1-O-CN**$^-$ with corresponding energies given in kcal/mol from DFT computations; see text for parameters used.

−100 °C. Our interpretation of this phenomenon is that over this temperature regime, even at room temperature, the $Fe(CO)_2(CN)$ unit is fixed, rendering each CO in distinct chemical environments because of the asymmetry in the pst bridge. This result is consistent with computational studies described below which find a high energy barrier for the $Fe(CO)_2(CN)$ rotation. The low temperature resonance broadening is likely due to slowing of the 3-carbon ring flip motion in the pst unit.

Scheme 3

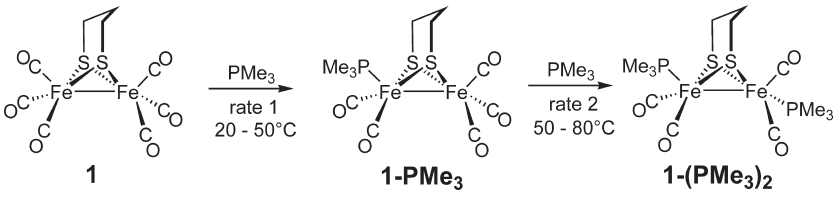

rate 1 = k_2 [**1**] [PMe_3] rate 2 = k_2' [**1-PMe$_3$**] [PMe_3]

Scheme 4

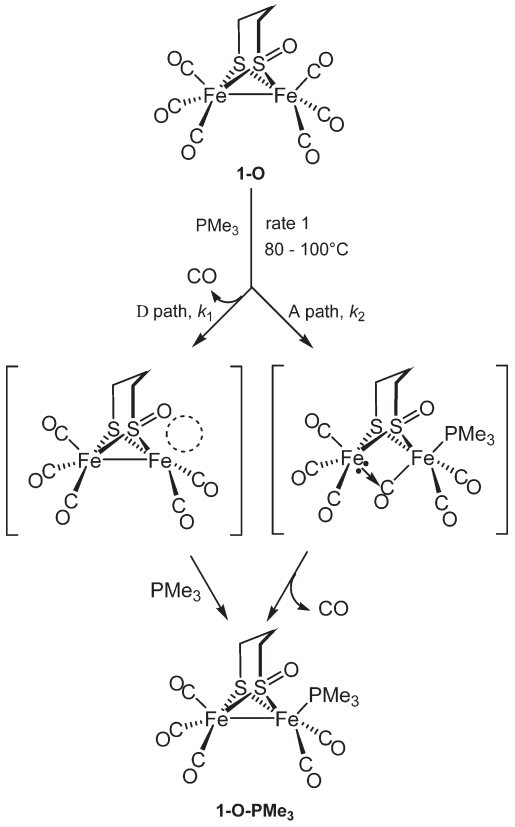

rate 1 = k_1 [**1-O**] + k_2 [**1-O**] [PMe_3]

The intramolecular, apical/basal CO exchange on individual $Fe(CO)_3$ units in the parent **1-O** complex ceases by −60 °C and has an activation barrier of ∼47 kJ/mol. In contrast, the same process in complex **1** has a barrier of 35 kJ/mol. A similar barrier, 33 kJ/mol, is found for the $Fe(CO)_3$ unit in the **1-O-CN**$^-$ complex. Thus, the deactivation effect of the pst bridge on rotation in the $Fe(CO)_3$ unit is counter balanced by the activating effect of the CN^- ligand on the adjacent iron.

Theoretical Results. To complement the experimental results, the intramolecular CO exchange process for **1-O-CN**$^-$ was explored by DFT computations. The optimized ground state and corresponding transition state structures en route to apical/basal CO exchange in the isomers of **1-O-CN**$^-$ are given in Figure 11.

The CN-apical conformation is the most stable ground-state isomer by about 4 kcal/mol as compared to the two CN-basal isomers. The activation barriers for both $Fe(CO)_3$ and $Fe(CO)_2CN$ rotation were calculated for all three isomers. Since similar results were obtained for the two CN-basal isomers, only the CN-basal isomer with cyanide cis to the S−O vector is given in Figure 11. The $Fe(CO)_3$ rotation barrier for the CN-apical isomer (Figure 11, (a)) is 6.06 kcal/mol, about 1.8 kcal/mol less than that required for the CN-basal isomer (Figure 11, (b)). The difference can be rationalized by better delocalization of the charge of the cyanide onto the bridging CO when the cyanide is in apical position and trans to the CO that migrates underneath the Fe--Fe bond vector. As indicated in Figure 11 by the metric data derived from the calculations, this is reflected by the Fe1−C1 distances and the greater bridging character of the CO that rotates under the Fe−Fe bond vector for the CN-apical isomer as compared to the CN basal isomer.

Consistent with conclusions from the VT ^{13}C NMR study, the $Fe(CO)_2CN$ unit rotation (Figure 11, (c) and (d)) requires a much higher energy—up to 19 kcal/mol. As suggested before, the orientation of the bridgehead carbon toward the rotated Fe site stabilizes the transition state (TS); the rotation barrier in (d) is about 3.7 kcal/mol less than that in (c). Note that the high energy TS structures correlate with almost linear CO's. For the CN-basal isomer, a rotated TS with cyanide underneath the Fe--Fe bond vector (Figure 11, (e)) was found to have a barrier of 22.8 kcal/mol. The Fe1C1N1 angle and the Fe2--C1 distance indicates the CN^- ligand has little interaction with Fe2 site.

Summary and Comments

A summary of the CO/PMe_3 reactivities of complexes **1** and **1-O** is given in Schemes 3 and 4. As noted above, the rate expressions for all reactions studied indicate associative processes. The expected increased electrophilicity of **1-O** over **1** toward PMe_3 was not realized; under identical conditions, the barrier to PMe_3 addition is higher for the former. For both **1** and **1-O**, the rate of PMe_3 nucleophilic attack on iron is slower for the second addition than for the first, consistent with diminished electrophilicity of the diiron unit after CO substitution with the first PMe_3 ligand. The **1-O** complex reacts much more sluggishly than **1**, leading into a temperature regime for practical measurements where CO dissociation competes with and obscures the associative path, Scheme 4. The addition of a second PMe_3 to **1-O-PMe$_3$** was so slow, even at elevated temperatures, that kinetic studies were not attempted.

The better nucleophilicity of CN^- as compared to PMe_3 is apparent in CO/CN^- substitutions in both **1** and **1-O**. Scheme 5 summarizes observations for the CO/CN^- exchange reactions. The kinetic studies established that in both **1** and **1-O** the individual CO/CN^- exchange steps proceed via associative paths; an elaborated version of Scheme 2 is shown

as Figure 12 specifically for the μ-pst complex. While the sequential step mechanism involving $Fe(CO)_3$ rotation concomitantly with CN^- nucleophilic attack on Fe holds for both, the reaction profiles differ in the relative values of E_{act} versus E'_{act}, Figure 13. The analysis of this switch in order invokes the contributing factors of nucleophilic attack, the $E_{act}(CN^-$ attack) of eq 1, and the coordination sphere fluxionality, the E_{act}(rot'n), of eq 1. As established by experiment from VT NMR studies, and corroborated by DFT computations, the rotational contribution for both complexes is lowered after the addition of the first CN^- ligand. For the μ-pdt complex this enhancement of rotation overwhelms the decrease in electrophilicity because of the negative charge of complex **1-CN**$^-$.[1] Because of the poorer donating ability of the S-oxygenate as compared to the thiolates, both μ-pst complexes, **1-O** and **1-O-CN**$^-$, are better electrophiles than the analogous μ-pdt complexes. However, they have significantly higher $Fe(CO)_3$ rotational barriers. Thus the decrease in electrophilicity in **1-O-CN**$^-$ is not counter balanced by an increase of fluxionality as it was in

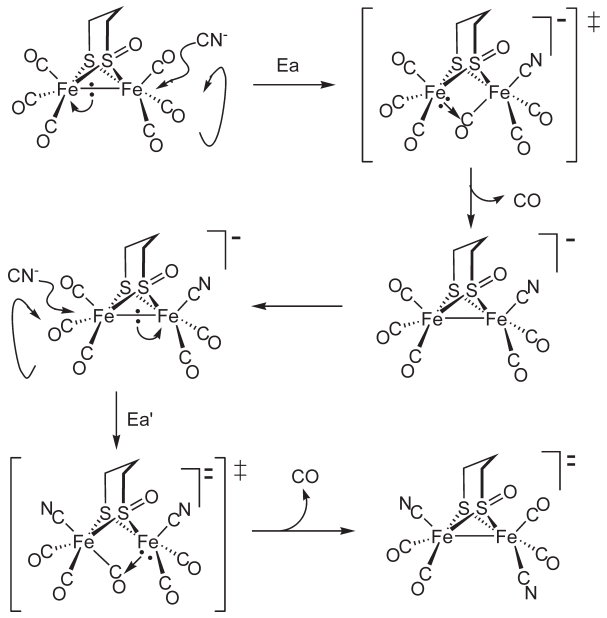

Figure 12. Mechanism for CN^-/CO exchange reaction in (μ-pst)[Fe$(CO)_3]_2$ (**1-O**).

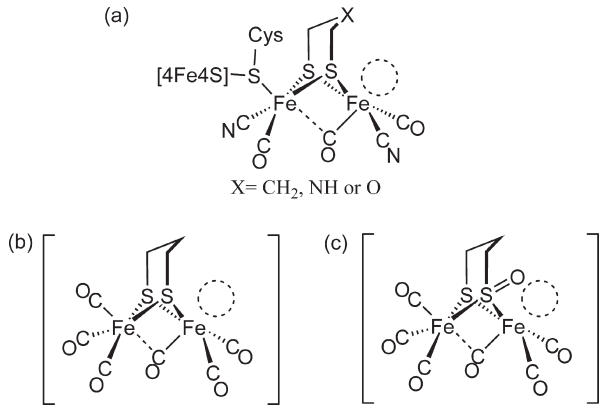

Figure 14. Structures of [Fe]H_2ase active site (a)[31,32] and transition state of $Fe(CO)_3$ rotation in (μ-pdt)[$Fe(CO)_3]_2$ (b),[1] and (μ-pst)[$Fe(CO)_3]_2$ (c).

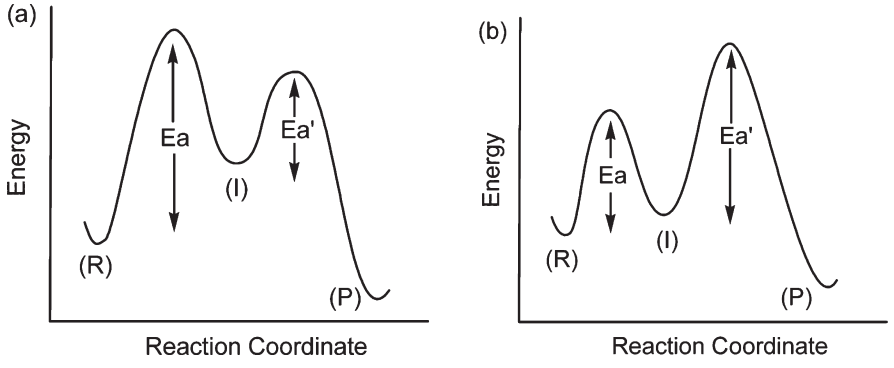

Figure 13. Reaction profiles of CN^-/CO substitution reaction of (a) (μ-pdt)[$Fe(CO)_3]_2$ (**1**) [1] and (b) (μ-pst)[$Fe(CO)_3]_2$ (**1-O**).

Scheme 5

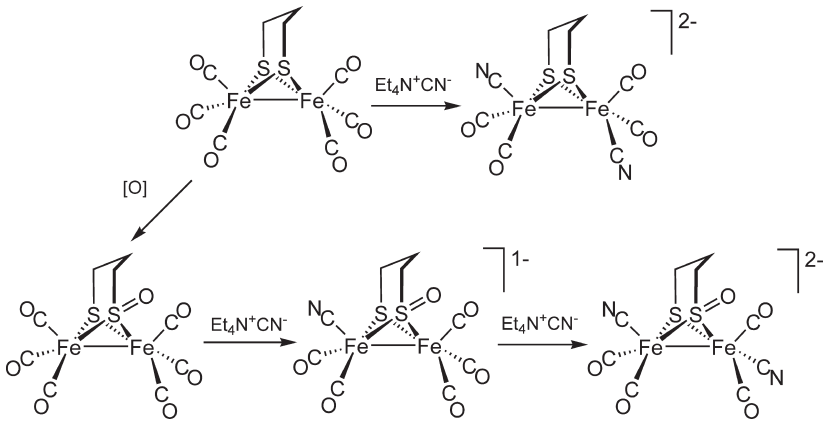

1-CN$^-$. This results in slower reaction rates and greater E_{act} barriers for the second CN^- substitution in **1-O-CN$^-$**.

While PMe_3 and CN^- have similar donor properties, kinetic studies find that "nature's phosphine", cyanide,[2,16] is a much better nucleophile in CO substitution reactions. The ligand dependence is additional evidence of the associative character of the mechanism of ligand substitution, noted in early studies of $(\mu\text{-SR})_2[Fe(CO)_3]$ to be rare examples of associative mechanisms in 6-coordinate metal complexes, the sixth position being held by the Fe−Fe bond.[27]

Comment on Relation to [FeFe] Hydrogenase Active Site. This work adds to a considerable literature which explores the features of $(\mu\text{-SRS})[Fe(CO)_3]_2$ as might explain the appearance of a modified version of this classic organometallic in nature, the diiron unit of the [FeFe]-H_2ase active site. The major conclusion from the current reactivity study is that the diiron construct is extremely sensitive to all conceivable modifications resulting from electronic tuning. Rarely has the potential for intramolecular structural fluxionality in a transition metal complex been so easily verified and so readily related to reactivity.

It is notable that the mixed-valent Fe^IFe^{II} diiron unit in the [FeFe]-H_2ase active site is in a ground state configuration that is "rotated" with respect to the ground state Fe^IFe^I complex structures of complexes **1** and **1-O**, Figure 14, *giving a geometry heretofore unknown in organometallic chemistry, yet synthetically accessed by the proper combination of donor/steric properties of ligands in a mixed valent, Fe ^{I} Fe ^{II} form.*[28−30] The transition state structures of **1** and **1-O** that apply to the CO site exchange process are also in the "rotated" diiron form, and such a geometry for the Fe^IFe^I diiron unit in the reduced redox level of [FeFe]-H_2ase active site would represent an "entatic state".[2] As earlier described in a "de novo" design approach to building diiron complexes,[4] an increase of electron density at the unrotated iron should stabilize the rotated transition state because of greater delocalization of electron density through the bridging carbonyl. This prediction was affirmed through CO/L substitution by better donating ligands.[4] The opposite case, a destabilization of the rotated transition state through removal of electron density, could not be experimentally established by CO ligand substitution. However, the modification of a thiolate to a sulfenate has this outcome, leading to a consistent view of the kinetic response of this unit to first coordination sphere effects: a reduction of electron density at iron diminishes the structural mobility of the diiron unit and its ability to expand the overall coordination number in the associative path to ligand substitution.

Acknowledgment. We acknowledge financial support from the National Science Foundation (CHE-0616695) and contributions from the R. A. Welch Foundation. The China Scholarship Council provided support for Bin Li. We appreciate helpful discussion with Prof. D. J. Darensbourg.

Supporting Information Available: Arrhenius plots for the formation of complex **1-PMe$_3$** from **1** and for the formation of **1-(PMe$_3$)$_2$** from **1-PMe$_3$**. Eyring plot and Arrhenius plot for the formation of **1-O-PMe$_3$** from **1-O**. Plot of $\ln(k_{obs})$ versus $\ln[PMe_3]$ for the formation of **1-PMe$_3$** from **1**, for the formation of **1-(PMe$_3$)$_2$** from **1-PMe$_3$** and for the formation of **1-O-PMe$_3$** from **1-O**. Plot of $\ln(k_{obs})$ versus $\ln[CN^-]$ for the formation **1-O-(CN)$_2^{2-}$** from **1-O-CN$^-$**. This material is available free of charge via the Internet at http://pubs.acs.org.

(27) Ellgen, P. C.; Gerlach, J. N. *Inorg. Chem.* **1973**, *12*, 2526–2532.
(28) Liu, T.; Darensbourg, M. Y. *J. Am. Chem. Soc.* **2007**, *129*, 7008–7009.
(29) Singleton, M. L.; Bhuvanesh, N.; Reibenspies, J. H.; Darensbourg, M. Y. *Angew. Chem., Int. Ed.* **2008**, *47*, 9492–9495.
(30) Justice, A. K.; Rauchfuss, T. B.; Wilson, S. R. *Angew. Chem., Int. Ed.* **2007**, *46*, 6152–6154.
(31) Popescu, C. V.; Munck, E. *J. Am. Chem. Soc.* **1999**, *121*, 7877–7884.
(32) Nicolet, Y.; de Lacey, A. L.; Vernede, X.; Fernandez, V. M.; Hatchikian, E. C.; Fontecilla-Camps, J. C. *J. Am. Chem. Soc.* **2001**, *123*, 1596–1601.